IEEE Access
Multidisciplinary | Rapid Review | Open Access Journal

Received July 5, 2021, accepted July 24, 2021, date of publication August 11, 2021, date of current version August 18, 2021.

Digital Object Identifier 10.1109/ACCESS.2021.3103969

Stochastic Geometry Analysis of Electromagnetic Field Exposure in Coexisting Sub-6 GHz and Millimeter Wave Networks

NOR AISHAH MUHAMMAD[1], NORHUDAH SEMAN[1], (Member, IEEE), NUR ILYANA ANWAR APANDI[2], CHUA TIEN HAN[1], YONGHUI LI[3,4], (Fellow, IEEE), AND OLAKUNLE ELIJAH[1], (Member, IEEE)

[1]Wireless Communication Centre, School of Electrical Engineering, Universiti Teknologi Malaysia (UTM), Johor Bahru, Johor 81310, Malaysia
[2]Faculty of Electrical Engineering, Universiti Teknikal Malaysia Melaka (UTeM), Durian Tunggal, Melaka 76100, Malaysia
[3]School of Electrical and Information Engineering, The University of Sydney, NSW 2006, Australia
[4]Peng Cheng Laboratory, Shenzhen 518055, China

Corresponding author: Nor Aishah Muhammad (noraishah.mhd@gmail.com)

This work was supported in part by the Ministry of Higher Education through the Fundamental Research Grant Scheme under Grant FRGS/1/2018/TK04/UTM/02/10, in part by the Higher Institution Centre of Excellence (HICoE) Grant under Grant 4J408, in part by Universiti Teknologi Malaysia (UTM) under Grant PDRU/04E90, and in part by the Ministry of Higher Education Malaysia through the Fundamental Research Grant Scheme by Universiti Teknikal Malaysia Melaka under Grant FRGS/2018/FKE-CERIA/F00355.

ABSTRACT The deployment of sub-6 GHz macro-cell networks, which are overlaid by millimeter-wave (MMW) small-cells, is a promising method to accommodate the unprecedented growth of data traffic demands and user devices. Although such a hybrid network could provide seamless connectivity and achieve high-quality services, there is a need to ensure that the growing number of base stations (BSs) does not affect biological safety, especially when the BSs are operated at high frequencies. This paper focuses on an analytical framework to investigate the electromagnetic field (EMF) exposure in a cellular network with coexisting sub-6 GHz and MMW BSs using a stochastic geometry approach. Locations of sub-6 GHz and MMW BSs are modeled as Poisson point processes (PPP). By incorporating different channel propagation, antenna, and fading models for sub-6 GHz and MMW tiers, the incident power density (IPD) coverage probability and the average IPD are derived and validated by Monte Carlo simulations. The impact of various system parameters such as BS density, number of antenna elements, and blockage density are investigated to gain insights on the network scenario. The results demonstrate that the variation of the EMF exposure level closely depends on the BS density and the number of antennas deployed at the BS. The results also show that the receiver sensitivity has a significant impact on the average IPD. For the same receiver sensitivity, it is revealed that an MMW user is exposed to a higher average IPD level than the sub-6 GHz counterpart. The results are also compared with the existing international regulations.

INDEX TERMS Electromagnetic field (EMF), millimeter wave, sub-6 GHz, stochastic geometry, Poisson point process, incident power density.

I. INTRODUCTION

With the rapid growth of wireless technologies, including the fifth-generation (5G) cellular networks, machine-to-machine (M2M) communications, and the internet of things (IoT), the demand for high network capacity, extremely high transmission speed and seamless connectivity have been escalated worldwide. Currently, there has been an increasing interest in deploying millimeter wave (MMW) small-cells underlying the conventional sub-6 GHz macro-cells to provide ample network capacity and ubiquitous coverage [1]. The sub-6 GHz network can provide universal coverage, but it encounters the spectrum shortage to support the substantial increase of wireless devices in the 5G and beyond 5G networks. Therefore, MMW communication, which uses the high segment of the frequency spectrum, e.g., 28 GHz and 73 GHz bands, will complement the sub-6 GHz network as it has the potential to provide multi-gigabit communication services due to the availability of huge bandwidth in the MMW spectrum.

The associate editor coordinating the review of this manuscript and approving it for publication was Miguel López-Benítez.

There are several unique features of MMW communications, making it different from the sub-6 GHz propagation. For example, MMW signals incur severe penetration loss, low diffraction, and scattering through blockages, resulting in a shorter link distance than the sub-6 GHz communication [2]. Moreover, the susceptibility of MMW propagation to blockage leads to very different path loss laws for the line-of-sight (LoS) and non-LoS links [3], [4]. Two key features of MMW cellular networks will be dense base station (BS) deployments and high directional transmissions at both BS and mobile. Adding BSs in a particular area can significantly boost the network capacity but produces more electromagnetic field (EMF) exposure in the surrounding environment. Furthermore, the beamforming technology with high directional antenna gain leads to a higher concentration of electromagnetic energy in a specific direction, which poses new issues when performing the EMF exposure assessment.

All BSs and wireless devices emit EMF, where the level of EMF needs to comply with the relevant regulatory requirements on human exposure. Despite the established exposure limits and safety standards by regulatory bodies such as International Commission on Non-Ionising Radiation Protection (ICNIRP) [5], International Electrotechnical Commission IEC-62232 [6], Federal Communications Commission (FCC) [7], and Institute of Electrical and Electronics Engineers IEEE [8], the EMF radiation in human and animal tissue has been, and continue to be, a public concern. The EMF exposure has received increasing interest in the past few years due to the rapid deployment of new BSs, especially the 5G technologies, to support the unprecedented capacity of the future wireless networks.

A. RELATED WORKS

There have been many research efforts on assessing the EMF exposure based on measurements [9]–[13] and simulations [14]–[16] in the past years. In general, the EMF exposure originates from two possible sources, i.e., (i) uplink signal from user equipment (UE), and (ii) downlink signal from BSs [17]. The former refers to the EMF in the near-field region and is commonly indicated by a specific absorption rate (SAR). Meanwhile, the latter refers to EMF exposure in the far-field region, which is measured based on the power density (PD) level. The measurement and characterization effort of EMF exposure from radio frequency (RF) devices started in the early 1990s, where the first version of ICNIRP guideline for the exposure limit to the electric, magnetic and electromagnetic field was provided in [18]. Such a guideline has served as a basis in many EMF studies, including the works in [9]–[13], [15]. The work in [9] provided a thorough discussion related to the issues and challenges in the EMF measurements of 5G networks. Among the key issue is the use of new techniques in 5G networks, such as massive MIMO and millimeter wave, which require the revision of EMF exposure assessment approaches.

Recently, several research works have been developed to characterize the RF EMF exposure on humans from cellular BSs [10]–[13], some of which incorporated the massive MIMO and MMW parameters. Specifically, the authors in [10] performed a real-site EMF measurement in the mid-city environment for the multiple BSs operated at 6 GHz to 18 GHz. The work in [11] focused on the impact of EMF exposure regulation in the planning phase of the 5G networks consisting of multiple locations of BSs operated at below 3 GHz. In [10] and [11], the authors found that the variation of the EMF level strictly depends on the communication environments and the adopted approach for measuring the EMF levels. Subsequently, the authors in [12] and [13] presented a comprehensive description of measurement methodology to assess the RF EMF exposure from 5G new radio (NR) BSs operated at sub-6 GHz and MMW bands. However, the measurements were obtained from a single transmitting node, and thus the results may not be accurate in multiple BS scenarios or dense networks. Since the 5G networks are not fully deployed, the RF EMF exposure assessment that incorporates new 5G features is still an open problem.

A simulation-based EMF exposure assessment has also received an increasing interest among the researcher and academia. The work in [14] presented an extensive system-level simulation to obtain the compliance boundary of massive MIMO BSs. The work in [15] compared the human exposure in terms of SAR and PD under different wireless technologies. Recently, the effect of massive MIMO on the EMF exposure has been further studied in [16], where the authors revealed that the pencil beamforming could be beneficial for network throughput and reduces the EMF level. However, the simulation studies in [14]–[16] considered the standard regular hexagonal model for BS locations, which is not sufficiently accurate for the current BS deployment that requires irregular network topologies. The irregular network topologies are due to the variation demand of network capacity and various communication environments, e.g., residential areas, high-rise buildings, and rural areas. While the system-level simulation is straightforward in design, it requires extensive computational time and resources, and it does not transparently provide insight into the system parameters. The lack of existing EMF assessment approaches has led to increasing interest in mathematical analysis. Compared to the EMF measurement, the mathematical model can provide an analytic prediction of the EMF exposure before the actual BS deployment.

Stochastic geometry is a useful mathematical and statistical tool for modeling and analyzing wireless networks with random topologies. This tool can provide a tractable analytical result where it has been widely applied to model and analyze the performance of wireless networks, including the 5G cellular networks [19]–[21], device-to-device communications [22], and energy harvesting networks [23]. However, all these works focused on common performance indicators such as signal-to-noise-plus-interference ratio (SINR), throughput, and energy efficiency. While the downlink and uplink analysis of such performance metrics are well understood by

now, more fine-grained analysis of EMF exposure, particularly at MMW frequency, is still an open issue.

To the best of our knowledge, there are very few discussions regarding the analytical study on the EMF exposure so far, except for recent work in [24]. However, there are several differences between our work and [24]. First, in [24], the authors considered a single tier MMW network, while in our work, a hybrid sub-6 GHz and MMW tiers are considered along with entirely different channel propagation, antenna, and fading models in each tier. Second, the work in [24] did not consider any cell association strategy in the analysis, while the maximum-biased received power (MRP) cell association strategy is adopted in our work, where all the BSs are assigned with an association bias value and the user is connected to a BS that has the strongest biased received power. Third, the global exposure metric considered in [24] is a different scope compared with our work. In [24], a global exposure, which is the summation of the received power from all BSs, was considered by using a fitted distribution of channel gain. In contrast, our work considers the distribution of incident power density (IPD) and the average IPD, which provide a more rigorous way to study the EMF exposure in a general system model instead of the site-specific scenario. Due to the differences in the system modeling, our analysis in this work is completely different from [24].

B. CONTRIBUTIONS

This paper analyzes the EMF exposure experienced by a user from a two-tier cellular network using a stochastic geometry framework. The main contributions of this paper are summarized as follows:

1) We present a mathematical framework for evaluating the EMF exposure in a cellular network with coexisting sub-6 GHz and MMW BSs by leveraging tools from stochastic geometry. The key factor that makes the EMF exposure analysis in hybrid networks distinct from other performance analyses is that the IPD depends on the total received power from BSs rather than the SINR, which serves as an indicator for the network reliability.
2) We present a detailed system model for coexisting sub-6 GHz and MMW networks and review the expressions of the relevant distance distributions, which serves as a basis for our analytical model. We consider two network cases, i.e., (i) a fully loaded network, representing a network with all active BSs, and (ii) a partially-loaded network, which refers to a network with a fraction of inactive BSs. Then, we characterize the IPD coverage probability of the typical user when the user equipment (UE) either connects to a sub-6 GHz BS or MMW BS. Using the IPD coverage probability expression in the two scenarios, we develop an expression for the average IPD of the typical user under hybrid networks.
3) To get a simpler IPD coverage probability expression, we consider a special environment case where a simplified blockage model is adopted. We develop an approximation of IPD coverage probability for dense MMW BS deployments.
4) Numerical results are provided to validate our mathematical analysis. We investigate the impact of system parameters, such as BS density, number of antenna elements, blockage density, and transmitted power on the IPD coverage probability and the average IPD. We also compare the analytical results with the existing exposure limit from ICNIRP [5] and FCC [7].

The rest of the paper is organized as follows. In Section II, the system model is introduced. The stochastic geometry analysis of the EMF exposure is provided in Section III. In Section IV, numerical and simulation results are presented to investigate the impact of system parameters on the EMF exposure. Finally, a conclusion is provided in Section V. A summary of notations is also provided in Table 1.

TABLE 1. Summary of notations.

Notation	Description
Φ_m,Φ_s	PPP of MBSs and SBSs
λ_m,λ_s	Intensities of MBSs and SBSs
Φ_u,λ_u	PPP and intensity of UEs
α_m, α_L α_N	Path loss exponents of sub-6 GHz MBS, LoS SBS and non-LoS SBS links
β	Blockage factor
f_m,f_s	MBS and SBS carrier frequencies
w_{f_m}, w_{f_s}	Wavelength of the sub-6 GHz and MMW frequencies=$(3 \times 10^8)/f_k$
δ_m,δ_s	Path loss intercepts of MBS and SBS
N_L,N_N	Nakagami fading parameter for LoS and non-LoS links
P_m, P_s	Transmit power of MBS and SBS
G_m,G_u	Antenna gain of MBS and UE
D	Dimension of antenna at sub-6 GHz BS
N_a	Number of antenna elements
D_a	Dimension of a single antenna element at MMW BS
G_1, G_2, θ_s	Main lobe gain, back lobe gain and main lobe beamwidth of the SBS antenna

II. SYSTEM MODEL

In this section, the spatial distribution of the sub-6 GHz and MMW BSs, antenna and channel models are introduced, followed by the cell association strategy. Then, we provide the definition of power density.

A. BASE STATION MODELING

We consider a two-tier network consisting of macro-cell base stations (MBSs) and small-cell base stations (SBSs) that are randomly distributed in a two-dimensional Euclidean space $\mathbb{R}^2$, as illustrated in Fig. 1. The MBS tier is operated at sub-6 GHz where the locations of the MBSs are modeled as a Poisson point process (PPP) $\{x_m\}^1 \equiv \Phi_m$ with intensity λ_m. Meanwhile, the SBS tier is assumed to operate at MMW where the locations of SBSs are distributed following another independent PPP $\{x_s\} \equiv \Phi_s$ with intensity λ_s. Mobile UEs are distributed independently following a homogeneous PPP Φ_u with intensity λ_u. Without loss of generality, the EMF

[1] Vectors in $\mathbb{R}^2$ are presented by bold lowercase letters.

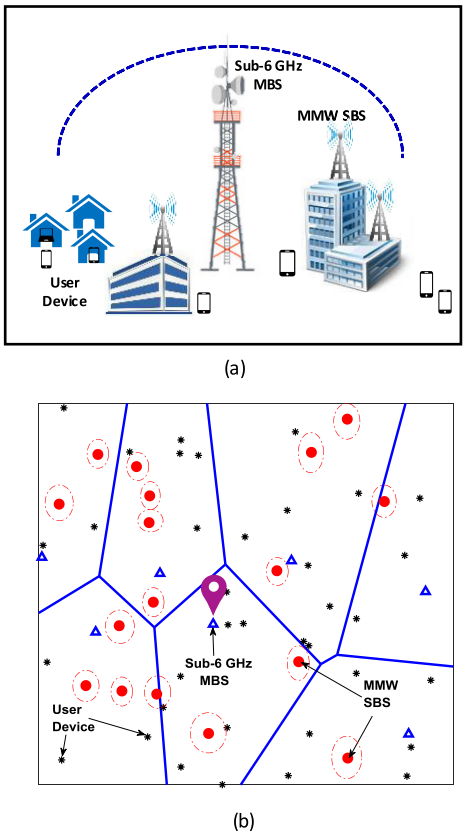

FIGURE 1. (a) An example of a cellular network with coexisting sub-6 GHz MBSs and MMW SBSs. (b) A realization of the sub-6 GHz MBSs and MMW SBSs using PPPs.

exposure analysis is performed on the typical outdoor UE, which is located at the origin.[2] For convenience, we denote the subscript $k \in (m, s)$ to represent the sub-6 GHz and MMW tiers, respectively.

In this paper, we assume that when multiple UEs are associated with a BS, the BS chooses a single UE in a round-robin fashion. It follows that only one UE in each BS is active at each time slot. We also assume that all the BS in the k-th tier transmit the same power in the downlink denoting by P_k.[3] Besides, we consider two network cases, i.e., fully loaded and partially loaded networks. In the former case, each BS has at least one UE to serve, where in practice, this case represents a scenario with more UEs than BSs. In the latter case, a BS may not have any user within its cell, and thus it is inactivated, meaning that this BS neither transmits nor generates interference. The latter case also can be regarded as ultra-dense networks in which there are more BSs than active users [26]. Let p_e^k represents the empty probability of the k-th tier, which corresponds to the probability that the base stations of the k-th tier are inactive. p_e^k can be approximated as [27]

$$p_e^k \approx \left(1 + \frac{\lambda_u}{3.5\lambda_k}\right)^{-3.5}. \tag{1}$$

From (1), the k-th tier network is considered as fully loaded when $p_e^k = 0$, whereas the k-th tier network is partially loaded if $p_e^k > 0$. From the thinning theorem [25], given p_e^k, the transmitting BSs in the k-th tier can be approximated as a PPP $\bar{\Phi}_k$ with intensity $\bar{\lambda}_k = (1 - p_e^k)\lambda_k$.

B. ANTENNA MODELING

We assume that all the sub-6 GHz MBSs are equipped with omnidirectional antennas with gain denoted by G_m. Meanwhile, directional antennas with sectored gain patterns as in [22] are adopted at all MMW SBSs. The antenna elements at an MMW SBS are denoted by N_a. The sectored antenna gain pattern is given as

$$G_s(\theta) = \begin{cases} G_1 = N_a & |\theta| \le \theta_s \\ G_2 = \dfrac{\sqrt{N_a} - \frac{\sqrt{3}}{2\pi} N_a \sin\left(\frac{\sqrt{3}}{2\sqrt{N_a}}\right)}{\sqrt{N_a} - \frac{\sqrt{3}}{2\pi} \sin\left(\frac{\sqrt{3}}{2\sqrt{N_a}}\right)} & \text{otherwise} \end{cases} \tag{2}$$

where G_1, G_2, and θ_s, are the main-lobe gain, side-lobe gain and main-lobe beamwidth, respectively, such that $\theta_s = \frac{\sqrt{3}}{\sqrt{N_a}}$. The user antenna gain also can be modeled in the same manner. However, for simplicity, each UE is assumed to have an omnidirectional antenna with antenna gain denoted by G_u.

A perfect beam alignment is assumed between the typical UE and its serving BS [28], [29], where the effective gain on the desired link is $G_1 G_u$. For the interfering BSs, we assume that each interferer is transmitting with the main-lobe beam pointed at a random direction. Thus, the steering angle of the interfering BSs is modeled as independently and uniformly distributed over $(0, 2\pi]$. In this case, the antenna gain of an interfering link is given by [29]

$$G_s = \begin{cases} a_1 = G_1 G_u & \text{wp } b_1 = \dfrac{\theta_s}{2\pi} \\ a_2 = G_2 G_u & \text{wp } b_2 = 1 - \dfrac{\theta_s}{2\pi} \end{cases} \tag{3}$$

where a_i is the probability distribution with probability (wp) b_i such that $i \in (1, 2)$.

C. PROPAGATION MODELING

1) BLOCKAGE MODELING

The effect of blockage is not prominent in the sub-6 GHz transmission signals since such signals have a high penetration capability and diffraction characteristics [4]. In contrast, the MMW signals are vulnerable to severe penetration losses, which lead to completely different path loss laws for LoS and non-LoS propagation. Following the work in [19], [20], [29], we consider a distance-dependent blockage model where an MMW link with distance r can be either in LoS or non-LoS state. The probability of LoS and non-LoS states are denoted respectively by $p_L(r) = e^{-\beta r}$ and $p_N(r) = 1 - e^{-\beta r}$, where β

[2]The notion of typicality is based on Slivnyak's theorem [25], which states that the statistics observed at a random point of a PPP is the same as that observed at the origin.

[3]In practice, the effect of EMF also dependent on the adaptive transmit power scheme and beamforming technique adopted by the BS. However, for practicality, the maximum transmitted power and perfect beam alignment are assumed for each BS.

is a parameter determined by the average size and the density of the blockages [19]. From the thinning theorem of PPP [25], the point process of MMW SBS, i.e., Φ_s can be divided into two independent and non-homogeneous PPPs, which are denoted by Φ_s^L and Φ_s^N with intensities, $\lambda_s p_L(r)$ and $\lambda_s p_N(r)$, respectively. Here Φ_s^L and Φ_s^N represents the point process of LoS SBSs and non-LoS SBSs, respectively.

2) SMALL-SCALE FADING

The small-scale fading of a link in the k-th tier is denoted by h_k. Rayleigh fading is commonly used to model the sub-6 GHz communications to capture rich-scattering environment [1] in which the small-scale fading for sub-6 GHz link, i.e., h_m, is assumed to follow an exponentially distributed with unit mean [28]. In contrast, Nakagami fading is assumed in MMW communications to exploit the sparse scattering nature of MMW channel [30]. The small scale fading for MMW is assumed as a normalized Gamma distribution such that $h_s \sim \Gamma(N, \frac{1}{N})$ with $N \in (N_L, N_N)$ is the Nakagami fading parameters [19], [23]. Here N_L and N_N are Nakagami fading parameters for LoS and non-LoS links, respectively.

Let $P_r^k(\mathrm{x}_k)$ denote the received power at the typical UE from a BS located at x_k in the k-th tier, which is given by [31]

$$P_r^k(\mathrm{x}_k) = P_k G_k G_u h_k \delta_k L_k(\mathrm{x}_k)^{-1}, \tag{4}$$

where $\delta_k = \left(\frac{w_{f_k}}{4\pi d_0}\right)^2$ is the path loss intercept with w_{f_k} is the wavelength of the frequency and d_0 is 1 meter reference distance. $L_k(\mathrm{x}_k) = ||x_k||^{\alpha_k}$ represents the path loss of the typical UE from a BS with distance $||\mathrm{x}_k||$, and α_k is the path loss exponent.

D. CELL ASSOCIATION

It is worth noting that the typical UE is assumed to be served by either a sub-6 GHz MBS or MMW SBS that is in LoS condition in order to guarantee the quality of service of the user. We consider the maximum biased received power association where the association probabilities are defined in the following definition.

Definition 1: The probability that the typical UE is associated with a sub-6 GHz MBS based on the maximum biased received power is defined as

$$\mathcal{A}_m = \mathbb{P}\left[P_m B_m G_m \delta_m L_{m,min}^{-1} > P_s B_s G_1 \delta_s L_{s,min}^{-1}\right], \tag{5}$$

whereas the probability that the typical UE is associated with a MMW SBS based on the maximum biased received power is defined as

$$\mathcal{A}_s = \mathbb{P}\left[P_s B_s G_1 \delta_s L_{s,min}^{-1} > P_m B_m G_m \delta_m L_{m,min}^{-1}\right], \tag{6}$$

where B_m and B_s refer to the bias value of the sub-6 GHz and MMW tiers, respectively.

E. POWER DENSITY

The incident power density (IPD) is a metric used to assess the EMF exposure in the far-field region.

Definition 2: The IPD is defined as the rate of energy flow per unit area, which is measured in watts per square meters (W/m^2) [17]. From (4), the IPD at the typical UE from a BS located at x_k is given by

$$S_k(x_k) = \frac{P_r^k(x_k)}{A_e} = \frac{P_k G_k h_k}{4\pi L(x_k)} \tag{7}$$

where $P_r^k(x_k)$ is given in (4) and $A_e = w_{f_k}^2 G_u/4\pi$ is the antenna effective area of the typical UE.

In general, the total IPD at any observation point is the sum of the energy coming from all the transmitting devices in the surrounding communication areas. Note that the IPD for sub-6 GHz and MMW tiers can be derived separately due to the orthogonality of both frequencies. In this paper, we analyze the IPD at the typical UE when it is served by a BS from k-th tier. Therefore, the total IPD at the typical UE with the serving BS at x^* in the k-th tier is given by

$$D_k(\mathrm{x}^*) = S_k(\mathrm{x}^*) + I_k, \tag{8}$$

where $S_k(\mathrm{x}^*)$ refers to the IPD from the serving BS in the k-th tier and is given in (7). I_k is the total IPD from the interfering BSs in the k-th tier, which is given by

$$I_k = \sum_{x_k \in \Phi_k \setminus x^*} \frac{P_k G_k h_k}{4\pi L(\mathrm{x}_k)}. \tag{9}$$

III. STOCHASTIC GEOMETRY ANALYSIS

In this section, we develop the mathematical model that characterizes the IPD of the two-tier network. We first provide the relevant distance distributions and the association probabilities that will be used in the subsequent analysis. Then, we derive the expressions for the IPD coverage probability of the sub-6 GHz and MMW networks, followed by the analysis of dense MMW networks.

A. DISTANCE DISTRIBUTION

Let R_m and R_s be the distance from the typical UE to the nearest sub-6 GHz MBS and the nearest MMW LoS SBS, respectively. The following lemmas provide the cumulative distribution function (CDF) and probability distribution function (PDF) of R_m and R_s.

Lemma 1: The CDF and PDF of the distance R_m, are respectively given as [32]

$$F_{R_m}(r_m) = 1 - \exp(-\pi \lambda_m r_m^2), \tag{10}$$

and

$$f_{R_m}(r_m) = 2\pi \lambda_m r_m \exp(-\pi \lambda_m r_m^2). \tag{11}$$

Lemma 2: The CDF and PDF of R_s, are respectively given by [33]

$$F_{R_s}(r_s) = 1 - \exp\left(-\frac{2\pi \lambda_s}{\beta^2}\left[1 - \frac{1+\beta r_s}{\exp(\beta r_s)}\right]\right), \tag{12}$$

and

$$f_{R_s}(r_s) = 2\pi \lambda_s r_s \exp\left(-\beta r_s - \frac{2\pi \lambda_s}{\beta^2}\left[1 - \frac{1+\beta r_s}{\exp(\beta r_s)}\right]\right). \tag{13}$$

Next, we characterize the cell association probabilities of sub-6 GHz and MMW tiers. Following the maximum biased received power in Section II-D, the typical UE can be served by either a MBS or a SBS. The expression of cell association probabilities for the sub-6 GHz and MMW tiers are provided in the following lemmas.

Lemma 3: The association probability of the typical UE to a sub-6 GHz MBS is given by

$$\mathcal{A}_m = \int_0^\infty [1 - F_{R_s}(k_m(r_m))]\, f_{R_m}(r_m) dr_m, \tag{14}$$

and the association probability to a LoS MMW SBS is

$$\mathcal{A}_s = \int_0^\infty [1 - F_{R_m}(k_s(r_s))]\, f_{R_s}(r_s) dr_s, \tag{15}$$

where $k_m(r_m) = \left(\frac{P_s B_s G_1 \delta_s}{P_m B_m G_m \delta_m}\right)^{\frac{1}{\alpha_s}} r_m^{\frac{\alpha_m}{\alpha_s}}$, $k_s(r_s) = \left(\frac{P_m B_m G_m \delta_m}{P_s B_s G_1 \delta_s}\right)^{\frac{1}{\alpha_m}} r_s^{\frac{\alpha_s}{\alpha_m}}$, $F_{R_m}(r_m)$, $f_{R_m}(r_m)$, $F_{R_s}(r_s)$ *and* $f_{R_s}(r_s)$ *are given in (10), (11), (12) and (13), respectively. Note that* $\mathcal{A}_s$ *can also be computed as* $\mathcal{A}_s = 1 - \mathcal{A}_m$ *[28].*

Proof: The proof of **Lemma 3** follows the same lines as given in [29, Appendix B]. □

Now, let X_k denotes the conditional distance that the typical UE associates with a BS in the k-th tier. We provide the PDF of the conditional distance in the next lemma.

Lemma 4: The PDF of X_m *conditioned on* $\mathcal{A}_m$ *given by*

$$f_{X_m}(x_m) = \frac{[1 - F_{R_s}(k_m(x_m))]}{\mathcal{A}_m} f_{R_m}(x_m), \tag{16}$$

and the PDF of X_s *conditioned on* $\mathcal{A}_s$

$$f_{X_s}(x_s) = \frac{[1 - F_{R_m}(k_s(x_s))]}{\mathcal{A}_s} f_{R_s}(x_s), \tag{17}$$

where $k_m(x_m)$, $k_s(x_s)$, $F_{R_m}(x_m)$, $f_{R_m}(x_m)$, $F_{R_s}(x_s)$ *and* $f_{R_s}(x_s)$ *are the same as provided in Lemma 3.*

Proof: The proof follows from that of [29, Lemma 4] and hence is skipped. □

B. POWER DENSITY ANALYSIS

As mentioned in Section II-E that the IPD is one of the metric used for the EMF exposure assessment from BSs. In this subsection, we provide the IPD distribution for the sub-6 GHz and MMW networks.

Definition 3: The IPD coverage probability is defined as the probability that the IPD experienced by the typical UE achieves the predefined threshold. The IPD coverage probability of the typical UE when it is tagged to a BS in tier k-th, is given by

$$\mathcal{E}_k(\gamma) = \mathbb{P}\left(D_k(x^*) > \gamma\right), \tag{18}$$

where γ *is the predefined IPD threshold, and* $D_k(x^*)$ *is given in (8). Note that* $\mathcal{E}_k(\gamma)$ *can also be interpreted as the complementary cumulative distribution function (CCDF) of IPD since the CDF is given by* $\mathbb{P}\left(D_k(x^*) \leq \gamma\right)$.

Now, we present the expressions of IPD coverage probability for both tiers in the next theorems.

Theorem 1: The IPD coverage probability given that the typical UE is associated with a sub-6 GHz BS can be tightly approximated as

$$\mathcal{E}_m(\gamma) \approx \sum_{v=0}^{V} (-1)^v \binom{V}{v} \int_{D_m}^\infty \left(1 + \frac{sP_m G_m}{4\pi x_m^{\alpha_m}}\right)^{-1} \mathcal{L}_m(x_m) \times [1 - F_{R_s}(k_m(x_m))] f_{R_m}(x_m) dx_m, \tag{19}$$

where

$$\mathcal{L}(x_m) = \exp\left(-2\pi \bar{\lambda}_m \frac{\epsilon x_m^{2-\alpha_m}}{\alpha_m - 2} \mathcal{G}(x_m)\right) \tag{20}$$

such that $\bar{\lambda}_m = (1 - p_e^m)\lambda_m$ *with* p_e^m *is given in (1), and* $\mathcal{G}(x_m) = {}_2F_1\left(1, 1 - \frac{2}{\alpha_m}, 2 - \frac{2}{\alpha_m}, -x_m^{-\alpha_m}\epsilon\right)$ *is the Gauss Hypergeometric function, and* $\epsilon = \frac{avP_m G_m}{4\pi\gamma}$. *In (19),* $D_m = 2D^2/w_{f_m}$ *represents the far-field Fraunhofer distance [17] with D represents the largest dimension of the antenna.* $s = \frac{av}{\gamma}$ *where v refers to the index of the Binomial expansion, and* $a = V(V!)^{-\frac{1}{V}}$ *with V is the parameter for the normalized Gamma random variable.* $F_{R_s}(\cdot)$ *and* $f_{R_m}(\cdot)$ *are given in (12) and (11), respectively.*

Proof: The proof is similar to that of [29, Appendix C]. However, for the reader's convenience, a simplified version is given in Appendix A. □

Theorem 2: The IPD coverage probability given that the typical UE is associated with a MMW BS can be tightly approximated as

$$\mathcal{E}_s(\gamma) \approx \sum_{v=0}^{V} (-1)^v \binom{V}{v} \int_{D_s}^\infty \left(1 + \frac{sP_s G_1}{N_L 4\pi x_s^{\alpha_L}}\right)^{-N_L} \times \mathcal{L}(x_s)\mathcal{N}(x_s)[1 - F_{R_m}(k_s(x_s))] f_{R_s}(x_s) dx_s, \tag{21}$$

where

$$\mathcal{L}(x_s) = \exp\left(-2\pi\bar{\lambda}_s \sum_{i=1}^{2} b_i \int_{x_s}^\infty Q_L^i(t) p_L(t) t dt\right), \tag{22}$$

$$\mathcal{N}(x_s) = \exp\left(-2\pi\bar{\lambda}_s \sum_{i=1}^{2} b_i \int_{x_s}^\infty Q_N^i(t) p_N(t) t dt\right), \tag{23}$$

$$Q_L^i(t) = 1 - \left(1 + \frac{sP_s a_i}{N_L 4\pi t^{\alpha_L}}\right)^{-N_L}, \tag{24}$$

$$Q_N^i(t) = 1 - \left(1 + \frac{sP_s a_i}{N_N 4\pi t^{\alpha_N}}\right)^{-N_N}. \tag{25}$$

such that $\bar{\lambda}_s = (1 - p_e^s)\lambda_s$, a_i *and* b_i *are given in (3) with* $i \in (1, 2)$. *In (21),* $D_s = 2N_a D_a^2/w_{f_s}$ *represents the far-field Fraunhofer distance [17] with* N_a *and* D_a *represent the number of antenna elements and the dimension of a single antenna element, respectively.* $F_{R_m}(\cdot)$ *and* $f_{R_s}(\cdot)$ *are given in (10) and (13), respectively.*

Proof: The proof is given in Appendix B. □

In contrast to the sub-6 GHz tier, the aggregate of the EMF exposure from interfering MMW SBSs is the summation of IPD generated by LoS MMW SBSs and non-LoS

MMW SBSs. Since the point process corresponds to LoS and non-LoS SBSs are independent, the Laplace transform of the sum of independent random variables can be written as the product of the individual Laplace transform as given in (21).

Remark 1: From (1), for any fixed user intensity (λ_u), the empty probabilities p_e^k in Theorem 1 and Theorem 2 increase as the BS intensity (λ_k) enlarges. Hence, the expression (20) in Theorem 1, and (22)-(23) in Theorem 2, which represent the total IPD of the interfering sub-6 GHz MBSs and MMW SBSs, respectively, converges to 1 as the $\lambda_k \to \infty$. Therefore, in partially-load networks, when $\lambda_k \gg \lambda_u$ the IPD is mainly contributed by the serving BS while the IPD from the interfering BSs can be neglected.

Next, we provide the analytical expression for the average IPD at the typical UE in the following proposition.

Proposition 1: The average IPD given that the user is associated to a BS in the k-th tier can be expressed as

$$\bar{\mathcal{E}}_k = \int_{\gamma}^{\infty} \mathcal{E}_k(x)dx + \gamma \mathcal{E}_k(\gamma), \tag{26}$$

where $\mathcal{E}_k(\gamma)$ is either given in (19) or (21), and $\gamma \in [\gamma_m, \infty)$ where γ_m is the minimum activation threshold.

Proof: The proof follows by assigning a non-negative value to γ, and the fact that $\mathcal{E}_k(\gamma)$ is the CCDF of γ [34]. Note that the use of activation threshold γ_m is needed to capture the radio-frequency receiver sensitivity [22]. □

C. IPD COVERAGE PROBABILITY OF DENSE MMW NETWORKS

In this subsection, we develop the IPD coverage probability of the typical UE for dense network scenario. Following the system performance analysis in [19], [35], the MMW network is expected to be densely deployed to achieve significant coverage. For such a scenario we consider a simplified LoS model in [19], where the LoS probability in Section II-C can be simplified as a step function $S_b(x)$, where $S_b(x) = 1$ if $0 < x < R_b$ and $S_b(x) = 0$, otherwise. Here, it is assumed that the typical UE has LoS condition to the BS in a fixed disc of radius R_b, where $R_b = \left(\frac{-\ln(1-\mathcal{A}_L)}{\pi\lambda_S}\right)^{0.5}$ with $\mathcal{A}_L$ is given in [19, Lemma 2]. The IPD coverage probability in Theorem 2 can be simplified by approximating the LoS probability with a step function and by further neglecting the small-scale fading. The expression of IPD coverage probability with simplified LoS probability is given in the following theorem.

Theorem 3: The IPD coverage probability for dense MMW networks is given by

$$\mathcal{E}_s(\gamma) \approx 2\pi\lambda_s \sum_{v=0}^{V} (-1)^v \binom{V}{v} \int_{D_s}^{R_b} \mathcal{W}(r)\mathcal{L}(r) \times \left[1 - F_{R_m}(k_s(r))\right] r \exp(-\pi\lambda_s r^2)dr, \tag{27}$$

where $\mathcal{W}(r) = \exp\left(-\frac{sP_s a_i}{4\pi r^{\alpha_L}}\right)$ and

$$\mathcal{L}(r) = \exp\left(-2\pi\lambda_s \sum_{i=1}^{2} b_i \int_{r}^{R_b} [1 - \mathcal{W}(t)]tdt\right). \tag{28}$$

Proof: The proof is provided in Appendix C. □

Remark 2: Note that the derivation approach in Theorem 3 is more tractable and much easier to numerically evaluate as the computation of Theorem 3 involves integration over a finite interval only.

IV. PERFORMANCE EVALUATION

In this section, simulation and numerical results are presented to validate the accuracy of the theoretical analysis. Monte Carlo simulations are considered for the system in a square area of 5 km x 5 km and the simulation results are obtained by averaging over 10^4 realizations. We generate the network with the first tier of randomly distributed sub-6 GHz BSs, followed by overlaying the MMW SBSs in the first tier, where both tiers are distributed as PPPs with the corresponding intensities. The typical user is located at the center of the simulation area. The propagation, antenna model, blockage model, and cell association are as described in Section II. The parameter values in Table 1 are employed in the simulation. Some parameters are changed in some figures to observe their impact on the IPD coverage probability and the average IPD.

A. VALIDATION OF THE ANALYTICAL MODEL

Fig. 2 plots the IPD coverage probability of the typical UE for various λ_s. The analytical results are obtained from Theorem 1 and Theorem 2 by using $V = 5$ terms of approximation.[4] In Fig. 2, we set the empty probability $p_e^m = p_e^s = 0$ to represent the fully-loaded networks. We also included in Fig. 2 the results based on analytical approximation in Theorem 3. Besides, to validate the IPD coverage probability for partially-loaded networks, we plot in Fig. 3 the IPD coverage probability of the typical UE for various N_a. Since the partially-loaded case occurs when the density of users is comparable or less than that of the BSs, i.e., $\lambda_u < \lambda_k$, and due to the fact that more SBSs are deployed in the future, we consider the empty probability in the MMW tier only where we set $p_e^m = 0$ and $p_e^s = (0.2, 0.8)$ in Fig. 3. It can be seen from both Fig. 2 and Fig. 3 that the simulation results closely match with the analytical results, which confirm the derived analytical expressions in Theorem 1 and Theorem 2. It is also seen in Fig. 2 that the approximation in Theorem 3 becomes tighter as the intensity of MMW SBSs increases. Hence, the approach for approximation in Theorem 3 is valid in very dense MMW BS deployments.

In addition, it is also observed from Fig. 2 that there is a contradicting trend between the IPD coverage probability in the sub-6 GHz and MMW tiers. When λ_s increases, the IPD coverage probability at the sub-6 GHz tier decreases, whereas

[4]Note that using more approximation terms, i.e, $V \geq 5$, leads to more accurate analytical results at the cost of longer computation time.

TABLE 2. Simulation parameters.

Notation	Value
λ_m,λ_s	5/km^2, 50/km^2 [28]
f_m,f_s	2 GHz, 28 GHz [20]
α_m, α_L,α_N	3, 2, 4 [28]
β	1/141.4 [19]
w_{f_m}, w_{f_s}	0.15, 0.0107 [36]
N_L,N_N	3, 2 [19]
P_m, P_s	46 dBm, 30 dBm [28]
G_m,G_u	0 dBi
D,D_a	7.5 cm [36], 0.3 cm [37]
N_a	32 [1]
ICNIRP	40 W/m^2 (2 GHz), 30.49 W/m^2 (28 GHz) [5]
FCC	10 W/m^2 [7]

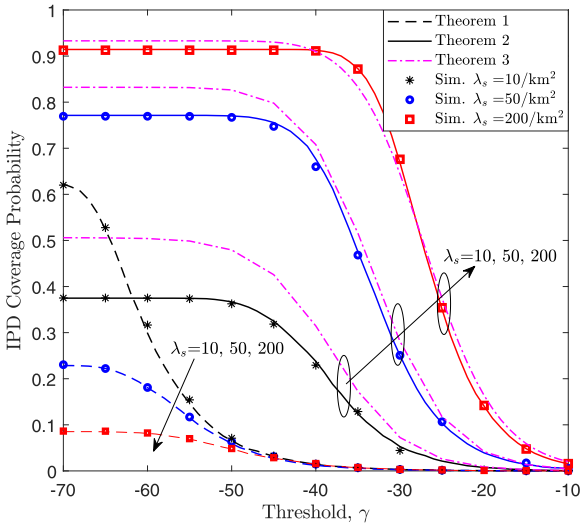

FIGURE 2. The IPD coverage probability of the fully-loaded networks for different MMW SBSs intensities λ_s. The dash lines, solid lines, and dash-dot lines are the IPD coverage probability obtained from Theorem 1, Theorem 2, and Theorem 3, respectively.

the IPD coverage probability at the MMW tier increases. This can be explained by the fact that the increasing MMW BS intensity λ_s leads to a lower distance from the typical UE to the nearest LoS MMW SBSs. Such a lower distance increases the likelihood that the typical UE connects to the MMW BS. Since from Lemma 3 we have $\mathcal{A}_s = 1 - \mathcal{A}_m$, increasing A_s will consequently decrease A_m.

B. EFFECT OF BASE STATION PARAMETER

Next, we plot in Fig. 4 and Fig. 5 the average IPD in the sub-6 GHz and MMW tiers, respectively. The analytical results are obtained from Proposition 1 using $V = 5$ and two values of the RF receiver sensitivity, i.e., $\gamma_m = -120$ dBm, and $\gamma_m = -90$ dBm. From Fig. 4 and Fig. 5, it is observed that the average IPD increases with the intensity of BSs. The intuitive reason is that when increasing the BS intensity, more BSs exist closer to the typical UE resulting in a shorter distance between the typical UE and the potential serving BS. From (7), it is seen that such a shorter link distance consequently increases the IPD from the serving BS. Moreover, this

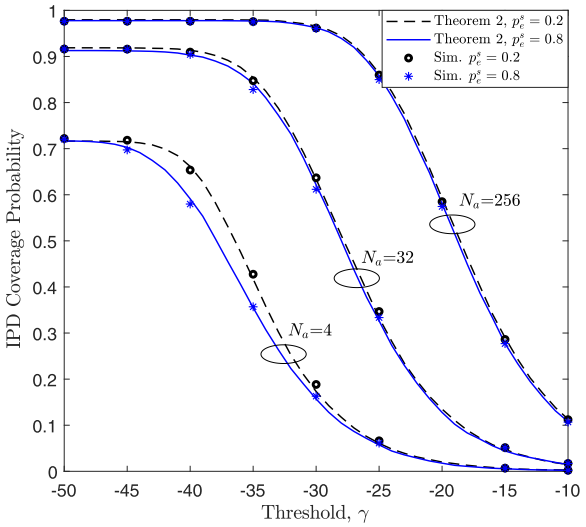

FIGURE 3. The IPD coverage probability of the partially-loaded networks for different number of BS antenna element N_a.

is due to the fact that more BSs in a particular area introduce more radiating sources, where it is observed from (8) that the additional BSs increase the total IPD from the interfering BSs and subsequently increases the EMF level at the typical UE. The results in Fig. 4 also demonstrate that the average IPD increases with the transmit power. This is because the IPD is directly proportional to the transmit power and thus increasing the transmit power at the BS generates more EMF exposure to the user.

In addition, in Fig. 4 and Fig. 5 the average IPDs are compared with the existing EMF standard limits from ICNIRP and FCC. The ICNIRP general public restrictions of IPD are 40 W/m^2 and 55/$f_s^{0.177}$, for frequency below 6 GHz and 6-300 GHz, respectively [5, Table 6]. Meanwhile, the maximum IPD for the frequency range of 1.5-300 GHz from the FCC guideline is 10 W/m^2 [7, Appendix A]. It is observed from both Fig. 4 and Fig. 5 that there is a significant difference between the average IPD with $\gamma_m = -120$ dBm and that of $\gamma_m = -90$ dBm. In this paper, γ_m is also regarded as the receiver sensitivity, which determines the minimum received signal that can be captured by the receiver. Decreasing the value of γ_m is equivalent to increasing the receiver sensitivity, where it can be seen in (26) that a smaller value of γ_m will increase the average IPD as the first term of (26) can be thought of as the computation of area within the CCDF region [34]. Therefore, the lower receiver sensitivity leads to a higher average IPD, which translates to a more accurate assessment of the EMF exposure.

Next, by comparing Fig. 4 and Fig. 5, it is noticed that under the same value of receiver sensitivity, the average IPD at MMW tier is higher than that in the sub-6 GHz tier. Besides, it is seen from Fig. 5 that the average IPD increases with the number of BS antenna elements. The reason is that the total gain of an antenna array is determined by the vector addition of the field radiated by the individual element [36]. Since in this work we have assumed that the main-lobe gain

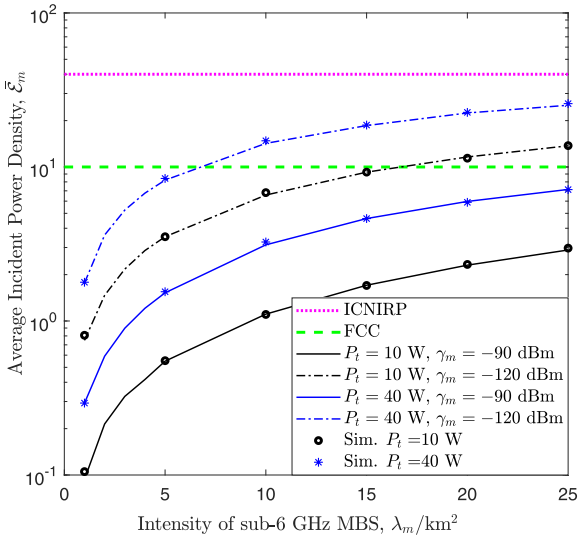

FIGURE 4. The average IPD as a function of λ_m. The solid lines and dash-dot lines are the average IPD obtained from Proposition 1 for $\gamma_m = -90$ dBm and -120 dBm, respectively.

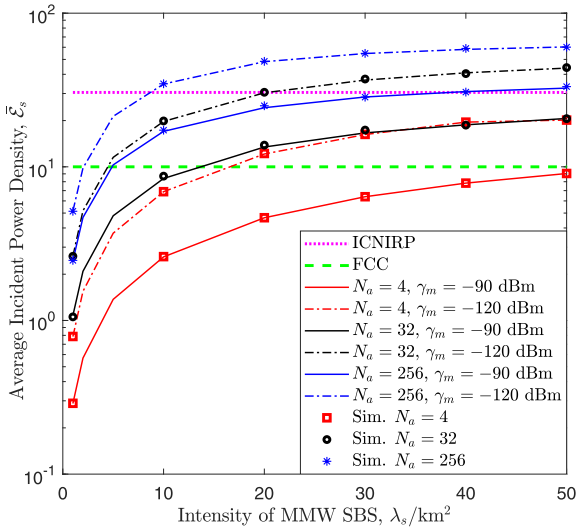

FIGURE 5. The average IPD as a function of λ_s. The solid lines and dash-dot lines are the average IPD obtained from Proposition 1 for $\gamma_m = -90$ dBm and -120 dBm, respectively.

equals to the number of antenna elements, i.e., N_a, increasing N_a leads to a higher main-lobe gain, which thus exposing the typical UE with stronger EMF and higher average IPD from the serving BS. Therefore, a proper selection of BS antenna element needs to be considered to ensure that the system complies with the EMF exposure limits.

C. EFFECT OF THE BLOCKAGE

Fig. 6 illustrates the IPD coverage probability of the typical UE for various blockage parameters β. It is seen from Fig. 6 that the IPD coverage probability of the typical UE at the MMW tier decreases with the blockage parameter β, whereas the IPD coverage at the sub-6 GHz tier increases with β. The intuitive reason is that the typical UE is more likely to

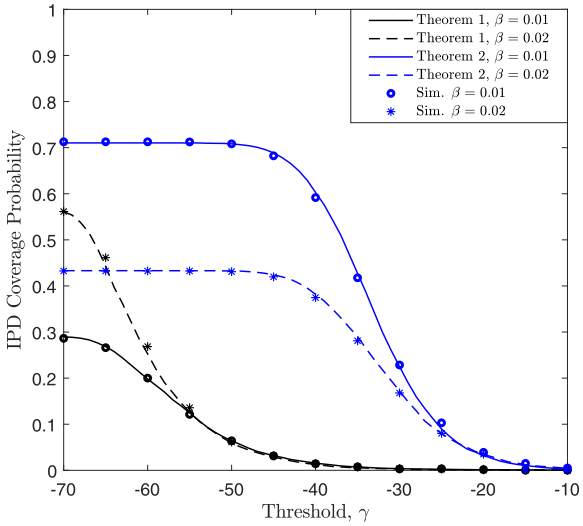

FIGURE 6. The IPD coverage as a function of β.

communicate with a LoS MMW SBS in an area with light blockage. In contrast, the association probability to the LoS MMW SBS decreases in the dense blockage areas because the MMW signal cannot penetrate the building. Moreover, the presence of blockages also can reduce the EMF from the interfering BS, which leads to the decreasing average IPD in dense building environments. On the other hand, the sub-6 GHz signal is less affected by blockage since it has a long wavelength and can penetrate easier through the blockage. In the hybrid network, the association probability to the MBS increases as the blockage parameter enlarges, which subsequently increases the average IPD at the sub-6 GHz tier.

V. CONCLUSION

This paper presented a mathematical framework for analyzing the EMF exposure in the coexisting sub-6 GHz and MMW cellular networks. We consider two scenarios network cases, i.e., fully-loaded network with all BSs in active states and partially-loaded network where only a fraction of inactive BSs. By using stochastic geometry tools, we investigated the effects of system parameters on the IPD coverage probability and the average IPD. The presented results showed that the IPD coverage probability and the average IPD increase with the increment of the BS intensity, i.e., λ_k, which subsequently increases the potential of EMF exposure. It is also found that the MMW tier contributes more EMF exposure to the user than the sub-6 GHz tier due to the use of directional antennas at MMW BSs. Moreover, the results demonstrated that the increasing number of antenna elements at MMW BSs leads to a stronger IPD. Also, it is revealed that a better receiver sensitivity will allow for an accurate EMF assessment. On the other hand, the presence of blockages could reduce the EMF from the interfering BSs. Findings in this paper will be useful for the analytic prediction of EMF exposure before the actual BS deployment to ensure a proper selection of the BS parameters in order to comply with the EMF exposure international regulations.

For future work, it would be interesting to consider the EMF exposure in the hotspot areas since MMW BSs will be deployed in highly populated areas to support the network capacity. From stochastic geometry perspective, this will necessitate the distribution of BSs and users generated by Poisson cluster processes (PCPs), which also incorporate the BSs and users coupling. Considering the EMF exposure in terms of the absorbed IPD in different human tissues, such as skin, fat and muscle, would also be of interest.

APPENDIX A
PROOF OF THEOREM 1

Let A_m be the event that the typical UE associate with the sub-6 GHz MBS. From (18), the IPD coverage probability of the typical UE when it is associated to the sub-6 GHz MBS located at x^* is given by

$$\begin{aligned}\mathcal{E}_m(\gamma) &= \mathbb{P}\left(D_m(\mathrm{x}^*) > \gamma, A_m\right)\\ &= \mathcal{A}_m \mathbb{P}\left(D_m(\mathrm{x}^*) > \gamma | A_m\right),\end{aligned} \tag{29}$$

where $\mathcal{A}_m$ is given in (14) and the second term of (29) is derived as

$$\begin{aligned}\mathcal{E}_m(\gamma) &= \mathbb{P}\left[D_m(\mathrm{x}^*) > \gamma \middle| A_m\right]\\ &\quad \times \mathbb{P}\left[S_m(\mathrm{x}^*) + I_m > \gamma \middle| A_m\right]\\ &\overset{(a)}{=} \mathbb{P}\left[g < \frac{S_m(\mathrm{x}^*) + I_m}{\gamma} \middle| A_m\right]\\ &\overset{(b)}{\approx} \mathbb{E}\left[\left(1 - \exp\left(-\frac{a(S_m(\mathrm{x}^*) + I_m)}{\gamma}\right)\right)^V \middle| A_m\right]\\ &\overset{(c)}{=} \sum_{v=0}^{V} (-1)^v \binom{V}{v} \mathbb{E}\left[\exp\left(s(S_m(\mathrm{x}^*) + I_m)\right) \middle| A_m\right],\end{aligned} \tag{30}$$

where (a) is obtained from (8) and by included a dummy random variable g, which follows a normalized Gamma with low variance, such that $g \sim \Gamma\left(V, \frac{1}{V}\right)$ with parameter V. (b) is from the CDF of g, where it can be tightly lower bounded as $\mathbb{P}[g < z] > (1 - e^{-az})^V$, with a constant $a = V(V!)^{-\frac{1}{V}}$ [23, Lemma 5]. (c) is obtained by using the Binomial expansion of (b) with $s = \frac{av}{\gamma}$.

The expectation in the last line of (30) can be given by

$$\begin{aligned}&\mathbb{E}\left[\exp\left(s(S_m(\mathrm{x}^*) + I_m)\right) \middle| A_m\right]\\ &\quad = \mathbb{E}\left[\exp(-sS_m(\mathrm{x}^*)) \mathbb{E}\left[\exp(-sI_m)\right] \middle| A_m\right]\end{aligned} \tag{31}$$

where the inner expectation in (31) is derived as

$$\begin{aligned}&\mathbb{E}\left[\exp(-sI_m)\right]\\ &\overset{(a)}{=} \exp\left(-2\pi\bar{\lambda}_m \int_{x_m}^{\infty} \left[1 - \left(1 + \frac{sP_mG_m}{4\pi t^{\alpha_m}}\right)^{-1}\right] tdt\right)\\ &\overset{(b)}{=} \exp\left(-2\pi\bar{\lambda}_m \frac{\epsilon x_m^{2-\alpha_m}}{\alpha_m - 2} \mathcal{G}(x_m)\right).\end{aligned} \tag{32}$$

where $\bar{\lambda}_m = (1 - p_e^m)\lambda_m$, (a) follows the similar step as in [32, (3)], and (b) is obtained by using Gauss hypergeometric function [38, p.1005] with $\mathcal{G}(x_m) = {}_2F_1\left(1, 1 - \frac{2}{\alpha_m}, 2 - \frac{2}{\alpha_m}, -(-x_m)^{-\alpha_m}\epsilon\right)$, and $\epsilon = \frac{avP_mG_m}{4\pi\gamma}$. Since the IPD is obtained at far-field region, we include $D_m = 2D^2/w_{f_m}$, which represents the far-field Fraunhofer distance [17] with D represents the largest dimension of the antenna.

Next, by substituting (32) in (31), and further evaluating the expectation of the combined expression with respect to S_m, we have

$$\begin{aligned}&\mathbb{E}\left[\exp\left(s(S_m(\mathrm{x}^*) + I_m)\right) \middle| A_m\right]\\ &\overset{(a)}{=} \int_{D_m}^{\infty} \left(1 + \frac{sP_mG_m}{4\pi x_m^{\alpha_m}}\right)^{-1} \exp\left(-2\pi\bar{\lambda}_m \frac{\epsilon x_m^{2-\alpha_m}}{\alpha_m - 2} \mathcal{G}(x_m)\right)\\ &\qquad \times f_{X_m}(x_m) dx_m,\end{aligned} \tag{33}$$

where the first term in (a) is obtained by using the moment generating function (mgf) of the exponential random variable, and $f_{X_m}(x_m)$ is given in (16). Finally, the expression in Theorem 1 is obtained from (33) with some algebraic simplification.

APPENDIX B
PROOF OF THEOREM 2

The derivation of Theorem 2 follows the same lines as in the proof of Theorem 1 in (30) except for the expression of the total IPD from interfering MMW BSs. In the MMW tier, the link between the typical UE and a SBS can be either in the LoS or non-LoS. From the thinning theorem of PPP [25], the point process of MMW SBS, i.e., Φ_s can be divided into two independent and non-homogeneous PPPs, which are denoted by Φ_s^L and Φ_s^N with intensities, $\lambda_s p_L(r)$ and $\lambda_s p_N(r)$, respectively. Here Φ_s^L and Φ_s^N represents the point process of LoS SBSs and non-LoS SBSs, respectively. Subsequently, we can derived the expression of the total IPD from interfering MMW BSs as

$$\mathbb{E}\left[\exp(-sI_s)\right] = \mathbb{E}\left[\exp(-sI_L)\right] \mathbb{E}\left[\exp(-sI_N)\right] \tag{34}$$

where I_L and I_N are the total IPD from LoS BSs and non-LoS BSs, respectively. The first term of (34), which is also the Laplace transform of interference caused by LoS MMW SBSs, is given by

$$\begin{aligned}&\mathbb{E}\left[\exp(-sI_L)\right]\\ &\overset{(a)}{=} \mathbb{E}\left[\exp\left(-s \sum_{x \in \Phi_s^L \setminus x^*} \frac{P_sG_sh_s}{4\pi |x|^{\alpha_L}}\right)\right]\\ &\overset{(b)}{=} \mathbb{E}\left[\prod_{x \in \Phi_s^L \setminus x^*} \left(1 + \frac{sP_sG_s}{N_L 4\pi t^{\alpha_L}}\right)^{-N_L}\right]\\ &\overset{(c)}{=} \exp\left(-2\pi\bar{\lambda}_s \sum_{i=1}^{2} b_i \int_{x_s}^{\infty} 1 - Q_L^i(t) p_L(t) t dt\right)\end{aligned} \tag{35}$$

where (a) is from (9), (b) is obtained by using the mgf of a normalized Gamma random variable with parameter N_L, and (c) follows from applying the probability generating functional (PGFL) of PPP Φ_s and the assumption that G_s is

a discrete random variable, where a_i and b_i are given in (3), and $Q_L^i(t) = 1 - \left(1 + \frac{sP_s a_i}{N_L 4\pi t^{\alpha_L}}\right)^{-N_L}$. The second term of (34) can be obtained following the similar steps as in (35).

Next, following the derivation steps in (33), and evaluating the expectation of the combined expression with respect to S_s, we obtain the IPD coverage probability of the typical UE in MMW tier as in Theorem 2.

APPENDIX C
PROOF OF THEOREM 3

The IPD coverage probability can be derived following the same steps in Appendix B. The only different is that the total IPD of interfering BSs is contributed by LoS MMW SBSs within the circular region of radius R_b. Subsequently, we approximate (34) as

$$\begin{aligned}
&\mathbb{E}\left[\exp(-sI_s)\right] \\
&\quad \approx \mathbb{E}\left[\exp(-sI_L)\right] \\
&\quad = \mathbb{E}\left[\exp\left(-s \sum_{x\in\Phi_s^L\cap[\mathcal{B}(0,R_b)\setminus x^*]} \frac{P_s G_s h_s}{4\pi |x|^{\alpha_L}}\right)\right] \\
&\quad \overset{(a)}{=} \exp\left(-2\pi\lambda_s \sum_{i=1}^{2} b_i \int_r^{R_b} 1 - \exp\left(-\frac{P_s G_s h_s}{4\pi t^{\alpha_L}}\right) t dt\right)
\end{aligned} \tag{36}$$

where $\mathcal{B}(0, R_b)$ represents the set of LoS MMW SBSs in a circular with radius R_b and (a) is obtained by neglecting the small-scale fading and using the PGFL of PPP Φ_s. The expression in Theorem 3 is obtained by further noting that the distance distribution of r simplifies to $f_R(r) = 2\pi\lambda_s r \exp(-\pi\lambda_s r^2)$ due to the LoS ball approximation.

REFERENCES

[1] J. G. Andrews, T. Bai, M. N. Kulkarni, A. Alkhateeb, A. K. Gupta, and R. W. Heath, Jr., "Modeling and analyzing millimeter wave cellular systems," *IEEE Trans. Commun.*, vol. 65, no. 1, pp. 403–430, Jan. 2017.

[2] T. Rappaport, S. Sun, R. Mayzus, H. Zhao, Y. Azar, K. Wang, G. Wong, J. Schulz, M. Samimi, and F. Gutierrez, "Millimeter wave mobile communications for 5G cellular: It will work!" *IEEE Access*, vol. 1, pp. 335–349, 2013.

[3] M. R. Akdeniz, Y. Liu, M. K. Samimi, S. Sun, S. Rangan, T. S. Rappaport, and E. Erkip, "Millimeter wave channel modeling and cellular capacity evaluation," *IEEE J. Sel. Areas Commun.*, vol. 32, no. 6, pp. 1164–1179, Jun. 2014.

[4] S. Rangan, T. S. Rappaport, and E. Erkip, "Millimeter-wave cellular wireless networks: Potentials and challenges," *Proc. IEEE*, vol. 102, no. 3, pp. 366–385, Mar. 2014.

[5] International Commission on Non-Ionizing Radiation Protection, "Guidelines for limiting exposure to electromagnetic fields (100 kHz to 300 GHz)," *Health Phys.*, vol. 118, no. 5, pp. 483–524, May 2020.

[6] *Determination of RF Field Strength, Power Density and SAR in the Vicinity of Radiocommunication Base Stations for the Purpose of Evaluating Human Exposure*, International Standard IEC 62232, International Electrotechnical Commission (IEC), 2017.

[7] *Evaluating Compliance With FCC Guidelines for Human Exposure to Radiofrequency Electromagnetic Fields. Supplement C (Edition 01-01) to OET Bulletin 65 (Edition 97-01)*, document OET Bulletin 65 (Edition 97-01), FCC, 1997. [Online]. Available: https://transition.fcc.gov/Bureaus/Engineering_Technology/Documents/bulletins/oet65/oet65c.pdf

[8] *IEEE Recommended Practice for Determining the Peak Spatial-Average Specific Absorption Rate (SAR) in the Human Head From Wireless Communications Devices: Measurement Techniques*, IEEE Standard 1528-2013, (Revision IEEE Std 1528-2003), 2013, pp. 1–246.

[9] R. Pawlak, P. Krawiec, and J. Z. urek, "On measuring electromagnetic fields in 5G technology," *IEEE Access*, vol. 7, pp. 29826–29835, 2019.

[10] R. Fernández-García and I. Gil, "Measurement of the environmental broadband electromagnetic waves in a mid-size European city," *Environ. Res.*, vol. 158, pp. 768–772, Oct. 2017. [Online]. Available: https://www.sciencedirect.com/science/article/pii/S0013935117308447

[11] L. Chiaraviglio, A. S. Cacciapuoti, G. D. Martino, M. Fiore, M. Montesano, D. Trucchi, and N. B. Melazzi, "Planning 5G networks under EMF constraints: State of the art and vision," *IEEE Access*, vol. 6, pp. 51021–51037, 2018.

[12] S. Aerts, L. Verloock, M. Van Den Bossche, D. Colombi, L. Martens, C. Törnevik, and W. Joseph, "*In-situ* measurement methodology for the assessment of 5G NR massive MIMO base station exposure at sub-6 GHz frequencies," *IEEE Access*, vol. 7, pp. 184658–184667, 2019.

[13] S. Adda, T. Aureli, S. D'Elia, D. Franci, E. Grillo, M. D. Migliore, S. Pavoncello, F. Schettino, and R. Suman, "A theoretical and experimental investigation on the measurement of the electromagnetic field level radiated by 5G base stations," *IEEE Access*, vol. 8, pp. 101448–101463, 2020.

[14] P. Baracca, A. Weber, T. Wild, and C. Grangeat, "A statistical approach for RF exposure compliance boundary assessment in massive MIMO systems," in *Proc. 22nd Int. ITG Workshop Smart Antennas (WSA)*, 2018, pp. 1–6.

[15] S. Kim and I. Nasim, "Human electromagnetic field exposure in 5G at 28 GHz," *IEEE Consum. Electron. Mag.*, vol. 9, no. 6, pp. 41–48, Nov. 2020.

[16] L. Chiaraviglio, S. Rossetti, S. Saida, S. Bartoletti, and N. Blefari-Melazzi, "'Pencil beamforming increases human exposure to ElectroMagnetic fields': True or false?" *IEEE Access*, vol. 9, pp. 25158–25171, 2021.

[17] Y. A. Sambo, F. Heliot, and M. A. Imran, "A survey and tutorial of electromagnetic radiation and reduction in mobile communication systems," *IEEE Commun. Surveys Tuts.*, vol. 17, no. 2, pp. 790–802, Oct. 2015.

[18] International Commission on Non-Ionizing Radiation Protection, "Guidelines for limiting exposure to time-varying electric, magnetic, and electromagnetic fields (up to 300 GHz)," *Health Phys.*, vol. 74, no. 4, pp. 494–522, 1998.

[19] T. Bai and R. W. Heath, Jr., "Coverage and rate analysis for millimeter-wave cellular networks," *IEEE Trans. Wireless Commun.*, vol. 14, no. 2, pp. 1100–1114, Feb. 2015.

[20] H. Ibrahim, H. Tabassum, and U. T. Nguyen, "The meta distributions of the SIR/SNR and data rate in coexisting sub-6 GHz and millimeter-wave cellular networks," *IEEE Open J. Commun. Soc.*, vol. 1, pp. 1213–1229, 2020.

[21] N. A. Muhammad, N. I. A. Apandi, Y. Li, and N. Seman, "Uplink performance analysis for millimeter wave cellular networks with clustered users," *IEEE Trans. Veh. Technol.*, vol. 69, no. 6, pp. 6178–6188, Jun. 2020.

[22] K. Venugopal, M. C. Valenti, and R. W. Heath, Jr., "Device-to-device millimeter wave communications: Interference, coverage, rate, and finite topologies," *IEEE Trans. Wireless Commun.*, vol. 15, no. 9, pp. 6175–6188, Sep. 2016.

[23] T. A. Khan, A. Alkhateeb, and R. W. Heath, Jr., "Millimeter wave energy harvesting," *IEEE Trans. Wireless Commun.*, vol. 15, no. 9, pp. 6048–6062, Sep. 2016.

[24] M. A. Hajj, S. Wang, L. T. Tu, S. Azzi, and J. Wiart, "A statistical estimation of 5G massive MIMO networks' exposure using stochastic geometry in mmWave bands," *Appl. Sci.*, vol. 10, no. 23, p. 8753, Dec. 2020.

[25] M. Haenggi, *Stochastic Geometry for Wireless Networks*. Cambridge, U.K.: Cambridge Univ. Press, 2013.

[26] M. Kamel, W. Hamouda, and A. Youssef, "Ultra-dense networks: A survey," *IEEE Commun. Surveys Tuts.*, vol. 18, no. 4, pp. 2522–2545, 4th Quart., 2016.

[27] S. Lee and K. Huang, "Coverage and economy of cellular networks with many base stations," *IEEE Commun. Lett.*, vol. 16, no. 7, pp. 1038–1040, Jul. 2012.

[28] H. Elshaer, M. N. Kulkarni, F. Boccardi, J. G. Andrews, and M. Dohler, "Downlink and uplink cell association with traditional macrocells and millimeter wave small cells," *IEEE Trans. Wireless Commun.*, vol. 15, no. 9, pp. 6244–6258, Sep. 2016.

[29] N. A. Muhammad, N. Seman, N. I. A. Apandi, and Y. Li, "Energy harvesting in sub-6 GHz and millimeter wave hybrid networks," *IEEE Trans. Veh. Technol.*, vol. 70, no. 5, pp. 4471–4484, May 2021.
[30] N. A. Muhammad, P. Wang, Y. Li, and B. Vucetic, "Analytical model for outdoor millimeter wave channels using geometry-based stochastic approach," *IEEE Trans. Veh. Technol.*, vol. 66, no. 2, pp. 912–926, Feb. 2017.
[31] A. Goldsmith, *Wireless Communications*, 1st ed. Cambridge, U.K.: Cambridge Univ. Press, 2005.
[32] J. G. Andrews, F. Baccelli, and R. K. Ganti, "A tractable approach to coverage and rate in cellular networks," *IEEE Trans. Commun.*, vol. 59, no. 11, pp. 3122–3134, Nov. 2011.
[33] C. Skouroumounis, C. Psomas, and I. Krikidis, "Low-complexity base station selection scheme in mmWave cellular networks," *IEEE Trans. Commun.*, vol. 65, no. 9, pp. 4049–4064, Sep. 2017.
[34] J. E. Freund, I. Miller, and M. Miller, *John E. Freund's Mathematical Statistics: With Applications*, 8th ed. London, U.K.: Pearson, 2004.
[35] J. Park, S.-L. Kim, and J. Zander, "Tractable resource management with uplink decoupled millimeter-wave overlay in ultra-dense cellular networks," *IEEE Trans. Wireless Commun.*, vol. 15, no. 6, pp. 4362–4379, Jun. 2016.
[36] C. A. Balanis, *Antenna Theory Analysis and Design*, 3rd ed. Hoboken, NJ, USA: Wiley, 2012.
[37] N. Ibrahim, T. A. Rahman, R. Ngah, O. A. Aziz, and O. Elijah, "Power density of rectangular microstrip patch antenna arrays for 5G indoor base station," *Indonesian J. Electr. Eng. Comput. Sci.*, vol. 19, no. 3, pp. 1367–1374, 2020.
[38] I. S. Gradshteyn and I. M. Ryzhik, *Tables of Integrals, Series, and Products*, 7th ed. San Diego, CA, USA: Academic, 2007.

NOR AISHAH MUHAMMAD received the B.Eng. and M.Eng. degrees in electrical engineering (telecommunications) from Universiti Teknologi Malaysia, Malaysia, in 2009 and 2012, respectively, and the Ph.D. degree from the School of Electrical and Information Engineering, The University of Sydney, Australia, in 2019. From 2009 to 2017, she was a Tutor at the Wireless Communication Centre (WCC), Universiti Teknologi Malaysia, where she has been a Postdoctoral Fellow, since 2019. From March 2011 to May 2011, she was a Visiting Researcher at the Computer Laboratory, University of Cambridge, U.K. She is currently a Senior Lecturer with the School of Electrical Engineering, Universiti Teknologi Malaysia. Her research interests include applications of stochastic geometry, millimeter wave and microwave communications, wireless propagation, channel modeling, and measurement.

NORHUDAH SEMAN (Member, IEEE) received the B.Eng. degree in electrical engineering (telecommunications) from Universiti Teknologi Malaysia, Johor, Malaysia, in 2003, and the M.Eng. degree in RF/microwave communications and the Ph.D. degree from The University of Queensland, Brisbane, St. Lucia, QLD, Australia, in 2005 and September 2009, respectively. In 2003, she was an Engineer with Motorola Technology, Penang, Malaysia, where she was involved in the RF and microwave components design and testing. She is currently an Associate Professor and the Director (Communication Engineering) of the School of Electrical Engineering and a Research Fellow with the HiCoE Wireless Communication Centre (WCC), Universiti Teknologi Malaysia. Her research interests include the design of microwave/millimeter wave devices for biomedical and industrial applications and effects of electromagnetic field radiation, including specific absorption rate (SAR) and power density and wireless communications.

NUR ILYANA ANWAR APANDI received the B.Sc. degree (Hons.) in industrial mathematics from Universiti Teknologi Malaysia (UTM), Malaysia, in 2002, the M.Sc. degree in modeling in applied mathematics from the University of East Anglia, Norwich, U.K., in 2004, and the Ph.D. degree from the School of Electrical and Information Engineering, The University of Sydney, Australia, in 2017. She is currently a Senior Lecturer at the Faculty of Electrical Engineering, Universiti Teknikal Malaysia Melaka (UTeM).

CHUA TIEN HAN received the B.Sc. degree (Hons.) in electrical engineering and the Master of Electrical Engineering degree in wireless engineering from the Universiti Teknologi Malaysia, in 2003 and 2007, respectively. From 2005 to 2007, he was a Tutor at the Faculty of Electrical Engineering, Universiti Teknologi Malaysia, where he has been a Lecturer, since 2007. His research interests include broadband fixed wireless access systems, radio propagation, channel modeling, and measurement.

YONGHUI LI (Fellow, IEEE) received the Ph.D. degree from Beijing University of Aeronautics and Astronautics, in November 2002. From 1999 to 2003, he was affiliated with Linkair Communications Inc., where he held a position of project manager with responsibility for the design of physical layer solutions for the LAS-CDMA system. Since 2003, he has been with the Centre of Excellence in Telecommunications, The University of Sydney, Australia, where he is currently a Professor with the School of Electrical and Information Engineering. His current research interests include wireless communications, with a particular focus on MIMO, millimeter wave communications, machine to machine communications, coding techniques, and cooperative communications. He holds a number of patents granted and pending in these fields. He was a recipient of the Australian Queen Elizabeth II Fellowship, in 2008, and the Australian Future Fellowship, in 2012. He received the Best Paper Awards from IEEE International Conference on Communications (ICC) 2014 and IEEE Wireless Days Conferences (WD) 2014. He has been on the organizing committees of several international conferences and a guest editor of several special issues. He is an Editor for IEEE TRANSACTIONS ON COMMUNICATIONS and IEEE TRANSACTIONS ON VEHICULAR TECHNOLOGY. He is an Executive Editor for *European Transactions on Telecommunications* (ETT).

OLAKUNLE ELIJAH (Member, IEEE) received the B.Eng. degree from the Federal University of Technology Minna, Minna, Nigeria, in 2003, the M.Sc. degree in micro-electronics and computing from Bournemouth University, Poole, U.K., in 2008, the master's degree in advance microelectronics from Bolton University, Bolton, U.K., in 2010, and the Ph.D. degree from Universiti Teknologi Malaysia, Johor Bahru, Malaysia, in 2018. He was a Field Engineer with Kuyet Nigeria Ltd., Lagos, Nigeria, in 2006. From 2011 to 2013, he was the MD/CEO with Mircoscale Embedded Ltd., Abuja, Nigeria. He is currently conducting research in the field of wireless communications and the IoT as a Postdoctoral Fellow with the Wireless Communication Centre, Higher Institution Centre of Excellence (HiCoE), Malaysia. His current research interests include embedded systems, wireless communication, massive MIMO, interference mitigation, heterogeneous network, the IoT with data analysis, and 5G.